

Investigation of Starting Characteristics with respect to Starting-Bar Shape in a Double-Cage Induction Motor

Gyeonghwan Yun, Yongha Choo, Changhwan Kim, and Cheewoo Lee*

Department of Electrical and Computer Engineering, Pusan National University, Busan 46241, Republic of Korea

(Received 24 November 2021, Received in final form 26 April 2022, Accepted 29 April 2022)

This paper presents the new shape of a rotor bar improving the starting performances in a double-cage induction motor (IM). The rotor bar of a double-cage IM is composed of a working bar, neck, and starting bar and each part has different effects on the characteristics of a motor. In this paper, it is confirmed that a starting bar has a dominant effect on the starting performances. The shape of a starting bar is designed by using the two ratios of the depth to width and the lower to upper width, respectively. The starting performances are closely analyzed by estimating the reactance and resistance of a rotor bar with respect to the depth through multi-layer method and FEA. Finally, by applying both the ratios to the starting bar, their mutual influence is scrutinized by using a response surface methodology and three models satisfying both starting torque and current aimed in this paper is proposed.

Keywords : shape of a starting bar, magnetic flux density distribution, rotor reactance and resistance, induction motor, starting torque and current, multi-layer method

1. Introduction

The starting performance of IMs is one of the most important factors in the design specifications of a motor. IMs have different torque-speed characteristics depending on the shape of a rotor slot and NEMA (National Electrical Manufacturers Association) classifies the shape of the rotor slot as 4 types according to the characteristics of a motor [1]. As the double-cage IM compared to other types has high starting torque and low starting current [2], the double-cage IM is mainly used to applications where the starting performance is important such as conveyors, crushers, stirrers, and compressors [3].

Various studies have been conducted to improving the characteristics of the double-cage IM. By using different materials for the upper and lower parts of a rotor bar, the performance of the motor is compared [4]. The design process of a working bar with high efficiency is proposed by using accurate coefficients instead of the empirical constants [5, 6]. However, the working bar mainly affects the characteristics at the nominal speed and the starting performance of an IM is determined by the starting bar

[7, 8]. To predict the performances of an IM, the equivalent circuit is composed of resistance and reactance calculated with the shape dimensions of the working and starting bar and the validity is verified by comparing the results of calculation by using the equivalent circuit and simulation [9, 10]. However, as the shapes of the working bar and starting bar are limited to a circle and rectangle, it is difficult to analyze characteristics with respect to the various shape.

In this paper, to improve the starting performance without any difference at the rated speed, the shape dimension of the starting bar is set as a variable under the same shape of the working bar. The shape of the starting bar is changed as following two ratios. One is the ratio of the depth to width and the other is the ratio of the lower to upper width of a starting bar. To scrutinize the starting performances depending on the shape of a rotor bar, the rotor shape and five parameters obtained through the multi-layer method and FEA are compared simultaneously. Five parameters in a rotor bar are given as below.

- 1) the reactance of a layer
- 2) the resistance of a layer
- 3) the equivalent reactance from the bottom to the corresponding position
- 4) the equivalent resistance from the bottom to the corresponding position

©The Korean Magnetism Society. All rights reserved.

*Corresponding author: Tel: +82-51-510-7377

e-mail: cwlee1014@pusan.ac.kr

5) the current flowing at the corresponding position

At the end of this paper, three objectives are set to improve starting performances and the new shape with two ratios is presented by using a Central Composite Design (CCD) in the Response Surface Methodology (RSM).

2. Starting Characteristic of Double Cage Induction Motor

2.1. Specification and operating characteristic in reference model

In this paper, a three-phase four-pole IM is selected as a reference model and the number of slots in a stator and rotor are 36 and 28, respectively. In Fig. 1, the cross-sectional view of the reference model and its specification

are given. The efficiency of the motor is 92.1 % satisfying more than the IE3 premium grade of 91.7 %. The rotor bar made of aluminum is divided into three parts and each part is called a working bar, neck, and starting bar.

Each part of the rotor bar has different effects on start-up and steady-state operations. In this paper, to identify the influence of each structure on the characteristics at the two operations, the distributions of current and magnetic flux are checked by using FEA. Fig. 2(a) and 2(b) show the distributions of current and magnetic flux when the motor starts (slip = 1), respectively. Fig. 2(c) and 2(d) show two distributions when the motor operates under the steady state (slip = 0.012). The color changes from blue to red as the magnetic flux density and current density increase. When the motor starts, it is confirmed that the

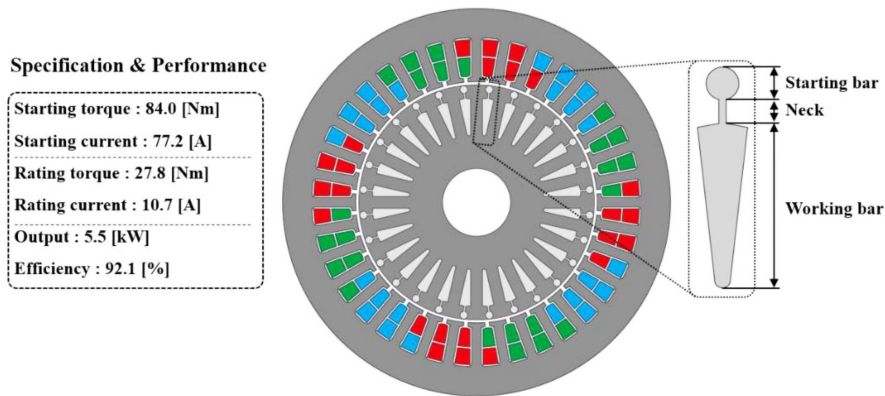


Fig. 1. (Color online) Cross-sectional view and specifications of reference model.

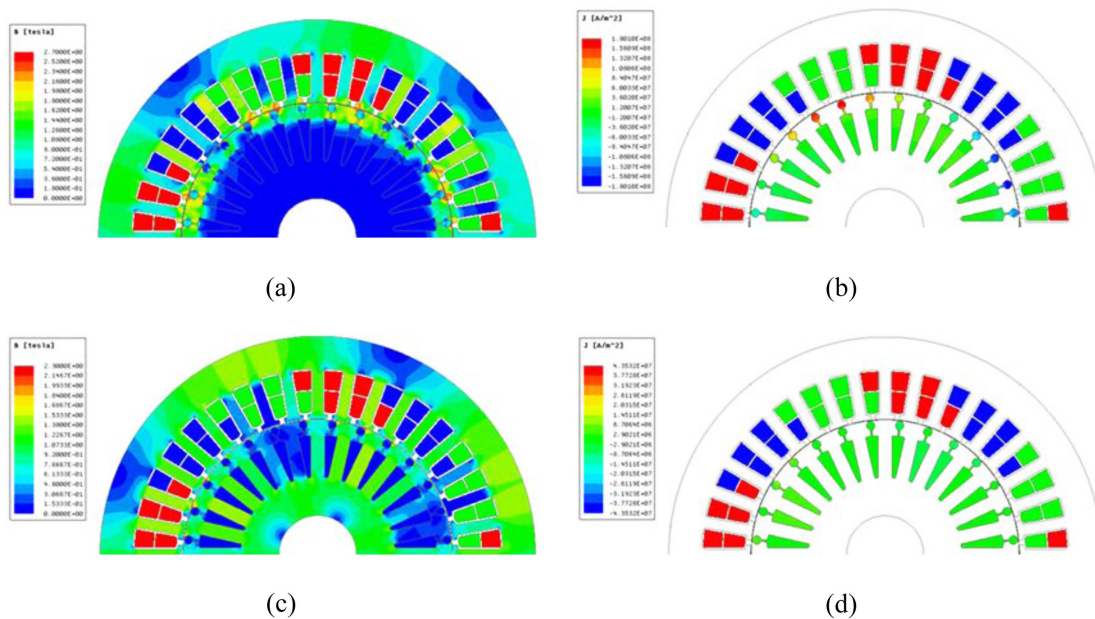


Fig. 2. (Color online) The distributions of current and magnetic flux: (a) the flux density in the slip = 1; (b) the current density in the slip = 1; (c) the flux density in the slip = 0.012; (d) the current density in the slip = 0.012.

magnetic flux is concentrated on the outside of the rotor and the current intensively flows in the starting bar. In contrast, in case of the steady state, the magnetic flux and current are evenly distributed to the rotor and rotor bar, respectively. The results from two operations mean that the influence of the starting bar on the starting performances is larger than the working bar due to the high leakage reactance when the motor starts. In this paper, to minimize the difference of characteristics between a proposed model and the reference model at the rated speed and to improve only the starting performance, the study is carried out by changing the shape of the starting bar with the same working bar and neck.

2.2. Starting torque and current in the induction motor

Figure 3 is the Thevenin equivalent circuit of the IM viewed from a rotor. The torque and current of the rotor are derived as shown in Eqs. (1) and (2) from the equivalent circuit.

$$I_r' = \frac{V_{sa}}{\sqrt{\left(R_s'' + \frac{R_r'}{S}\right)^2 + (X_{ls}'' + X_r')^2}} \quad (1)$$

$$T = \frac{3}{\omega_s} \frac{R_r'}{S} I_r'^2 = \frac{3}{\omega_s} \frac{V_{sa}^2 \frac{R_r'}{S}}{\left(R_s'' + \frac{R_r'}{S}\right)^2 + (X_{ls}'' + X_r')^2} \quad (2)$$

here, V_{sa} , S , ω_s , R_s'' , X_{ls}'' , R_r' , and X_r' are voltage, slip, angular velocity, the resistance of the stator, the reactance of the stator, the resistance of the rotor, and the reactance of the rotor, respectively. The torque and current when the motor starts are expressed as Eqs. (3) and (4).

$$I_{r|s=1}' = \frac{V_{sa}}{\sqrt{(R_s'' + R_r')^2 + (X_{ls}'' + X_r')^2}} \quad (3)$$

$$T_{start|s=1} = \frac{3}{\omega_s} \frac{V_{sa}^2 R_r'}{(R_s'' + R_r')^2 + (X_{ls}'' + X_r')^2} \quad (4)$$

When the IM starts, the current flowing through the

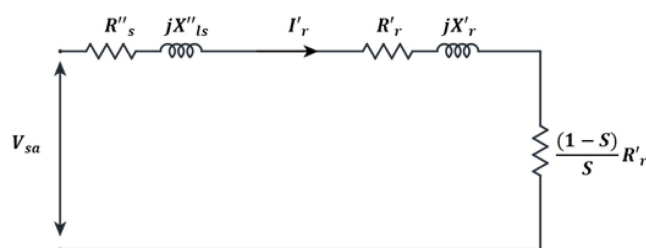


Fig. 3. Thevenin equivalent circuit of squirrel induction motor.

rotor bar is concentrated on the starting bar due to the skin effect. The effective area where the current flows is changed and the resistance R_r' in consideration of the effective area is changed. Therefore, to improve the starting performance of the induction motor, it is necessary that the resistance and reactance of the rotor considering the skin effect is quantified [11-13]. In this paper, the impedance of the rotor is calculated through the multi-layer method. The multi-layer method means that an object is divided into a lot of micro pieces and the parameters of each piece are calculated. The advantages of the method are having few restrictions on the shape of an object and reflecting the skin effect.

2.3. Impedance calculation of rotor bar through the multi-layer method

Figure 4 shows a multi-layered rotor bar and its equivalent circuit. The resistance and reactance of the p^{th} piece having height h_p and width b_p are calculated by Eqs. (5) and (6).

$$r_p = \frac{\rho l_{stack}}{b_p h_p} \quad (5)$$

$$X_p = S \omega_e \mu_0 \frac{l_{stack} h_p}{b_p} \quad (6)$$

To obtain the resistance and reactance of a rotor bar, arbitrary current is substituted with I_1 and the voltage of a rotor bar is calculated by Eq. (7).

$$V_{bar} = r_n I_n + j X_n I_{bar} \quad (7)$$

The impedance of the rotor bar is calculated by Eq. (8) with V_{bar} and I_{bar} , where the real part is the resistance and the imaginary part is the reactance.

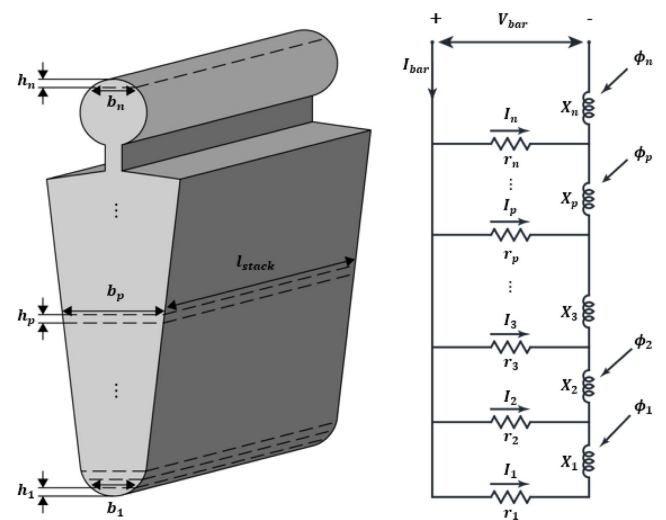


Fig. 4. Rotor bar and equivalent circuit with multilayer.

$$Z_{bar} = \frac{V_{bar}}{I_{bar}} = R_{bar} + jS\omega_e L_{bar} \quad (8)$$

In this paper, the multi-layer analysis is performed with the same height h_p for all models.

3. Analysis of Starting Performances Based on Rotor Bar Shape

Various studies have been conducted in the direction of improving the starting performance of a squirrel cage IM by changing the shape of a rotor bar. The starting performances are improved by controlling the ratios of the depth to width and the lower to upper widths of the rotor bar in the squirrel cage induction motor [14, 15].

However, since the double squirrel cage induction motor consists of the working bar, neck and starting bar, it is difficult to adopt the previous research. In this paper, the two ratios of depth to width and lower to upper width are applied to the starting bar. Fig. 5 shows the two types of the starting bar and Eq. (9) is the ratio k used in this study.

$$k = \frac{b}{a} \quad (9)$$

In case of a type1 having depth a and width b , the depth decreases and the width increases as much as the ratio k increases. When the ratio k of a type2 having upper depth a and lower depth b with fixed width h increases, the width of the upper part is wider than the width of the

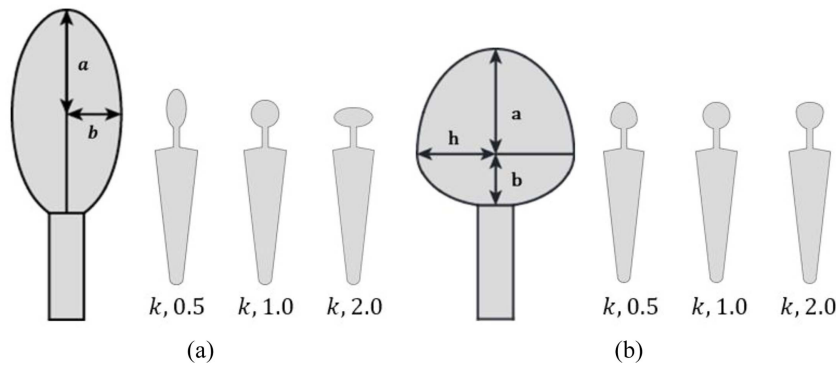


Fig. 5. Shape of rotor bar: (a) type 1; (b) type 2.

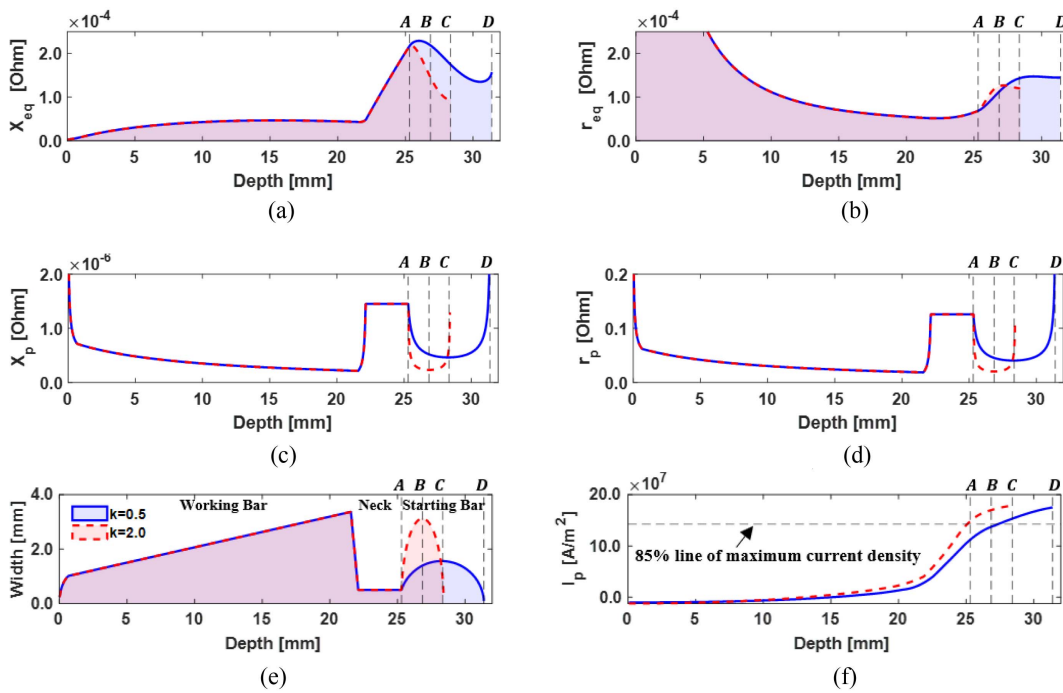


Fig. 6. (Color online) Parameters of Type 1 calculated by multilayer method: (a) equivalent reactance; (b) equivalent resistance; (c) reactance; (d) resistance; (e) width; (f) current density.

lower part. The shape of the starting bar in case of $k = 1$ is the same as the reference model regardless of the type. To identify the relationship between the starting-bar shape and the starting characteristics, the study is divided into two stages. First, by studying the two types of starting bar individually, the direct effect of the change of the starting-bar shape on the starting performances is investigated. Second, this study proposes a newly designed model type having the characteristics of both two types, and three models with improved starting performances are exhibited by using the RSM at the end.

3.1. Relationship between ratio of depth to width and starting performances

Each parameter calculated through the multi-layer method and FEA for the type1 is shown in Fig. 6. The parameters for two models ($k = 0.5$ and $k = 2.0$) are compared and shown by a blue solid line and a red dotted line, respectively. Fig. 6(a) and 6(b) are the equivalent reactance X_{ea} and resistance r_{eq} from the bottom of a rotor bar to the corresponding position. Fig. 6(c) and 6(d) are the reactance X_p and resistance r_p calculated by Eqs. (5) and (6). Fig. 6(f) shows the current flowing at the corresponding position and the 85 % point of the maximum current is shown with a dotted line. Fig. 6(e) shows the shape of the rotor on the same x-axis for the intuitive comparison with other parameters.

As shown in Fig. 6(e), since the working bar and neck for the two models have the same dimensions, X_{ea} , r_{eq} , X_p , and r_p up to point A do not differ between models. Unlike the working bar and starting bar, the neck having a thin width has a large value in X_p and X_{eq} up to point A is greatly increased. Due to the large value of X_p in the neck, the current flowing through the working bar and neck is limited as shown in Fig. 7. As a result, the effective area where the current flows is reduced and the resistance

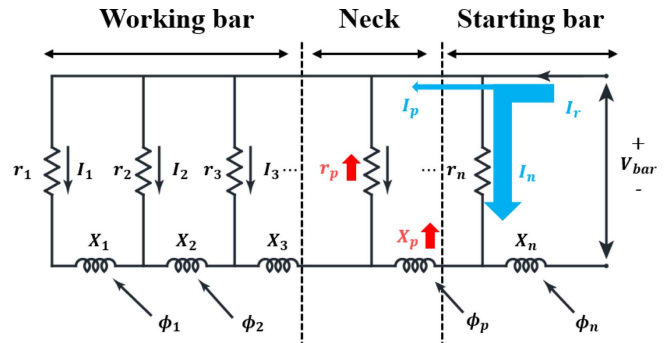


Fig. 7. (Color online) Current flow when the motor starts.

considering the effective area is increased. Hereafter, this effect is referred to as “the neck effect” in this paper.

As shown in Fig. 6(c) and 6(e), each reactance X_p , which is inversely proportional to the width b_p , is reduced and increased according to width. The reactance X_p of one model ($k = 2.0$) having the large rate of change in width after point A is greatly reduced and X_{eq} immediately decreases according to the change of X_p . On the other hand, in the case of the other model ($k = 0.5$), the peak of X_{eq} is generated between points A and B, not point A. It means that the narrow lower part of the starting bar has the same effect as the neck effect. As a result, the 85 % point of the maximum current density for the model ($k = 0.5$) is located at point B, higher position than the model ($k = 2.0$), and the total current flowing through a rotor bar is smaller than the model ($k = 2.0$).

Figure 8(a) shows the resistance R_r' and reactance X_r' of a rotor with respect to k for type 1. Starting torque and current are shown in Fig. 8(b). When the depth decreases and the width increases, the reactance and resistance of the rotor bar are decreased by 29.5 % and 16.8 %, respectively. As both the resistance and reactance decrease, the starting torque and current are increased.

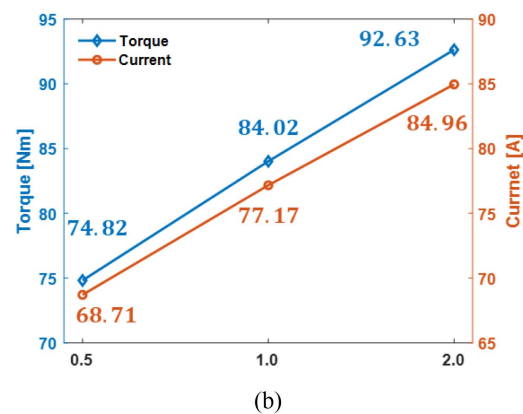
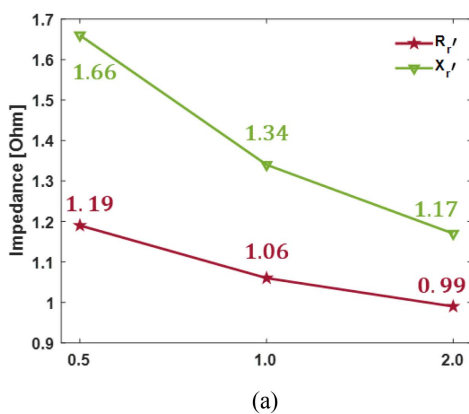


Fig. 8. (Color online) Parameters with respect to k for type 1: (a) resistance and reactance of a rotor; (b) starting torque and current.

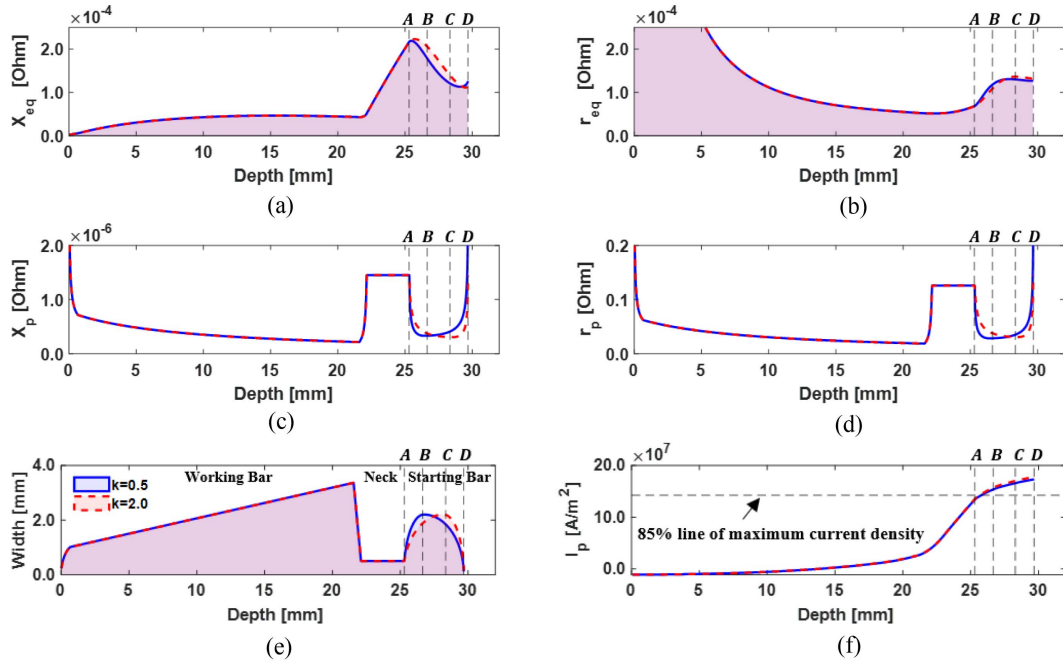


Fig. 9. (Color online) Parameters of Type 2 calculated by multilayer method: (a) equivalent reactance; (b) equivalent resistance; (c) reactance; (d) resistance; (e) width; (f) current density.

3.2. Relationship between ratio of lower to upper width and starting performances

Each parameter calculated through the multi-layer method and FEA for Type2 is shown in Fig. 9. One model ($k = 0.5$) has a wide lower part and the other model ($k = 2.0$) has a wide upper part as shown in Fig. 9(e). In case of the model ($k = 2.0$), the narrow lower part of starting bar is worked like a neck and the current is concentrated on the upper part of the rotor bar due to the neck effect at the lower part. When the current is concentrated on the upper part, the effective area is reduced and the resistance is increased. The phenomenon that the resistance of the model with the narrow lower

part is increased is same as type 1. However, unlike the type 1 having up and down symmetrical shape, the model ($k=0.5$) with the wide lower part in type 2 has large value in X_p at the end point (Point D) due to the narrow upper part.

Figure 10 shows R_r' , X_r' , the starting torque, and current with respect to k for type 2. In case of Type 2 having no difference of depth between models, there is little difference in the resistance and reactance with respect to ratio k compared to type 1, but one model ($k = 2.0$) with 5.8 % lower reactance has 2.9 % larger resistance than the other model. By the increased the resistance and decreased reactance, the starting torque is

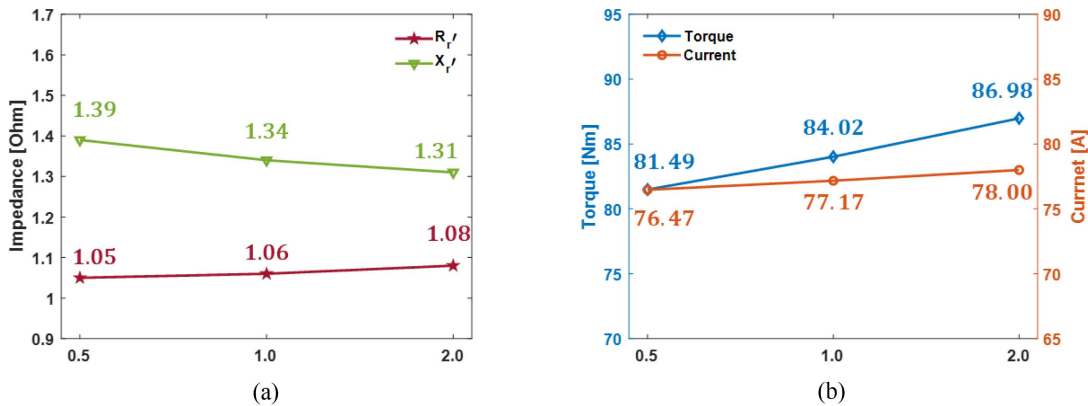


Fig. 10. (Color online) Parameters with respect to k for type 2: (a) resistance and reactance of a rotor; (b) starting torque and current.

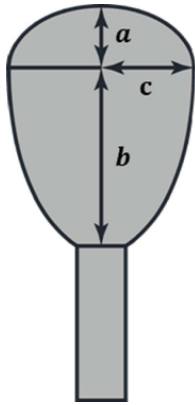


Fig. 11. New shape of starting bar by considering two ratios.

greatly increased by 6.7 % compared to the 2 % increased starting current. As shown in Fig. 8 and Fig. 10, It is noted that the two ratios used in this paper are key factors in varying the resistance and reactance of the rotor bar when motor starts.

4. Proposed Model with Improved Starting Performances

In this section, three models satisfying the starting performances set up in this paper are presented by using the CCD. Fig. 11 shows the new shape of the starting bar designed by considering both two ratios, and the ratios of depth to width ($K_{D/W}$) and lower to upper width ($K_{L/U}$) are expressed as Eqs. (10) and (11).

$$K_{D/W} = \frac{2c}{a+b} \tag{10}$$

$$K_{L/U} = \frac{b}{a} \tag{11}$$

When $K_{D/W}$ increases to 2 or more, it is confirmed that the starting current is increased by more than 10 % in comparison with the reference model as shown in Fig. 8. Increased $K_{L/U}$ greatly increases the starting torque compared to the starting current as shown in Fig. 10. Therefore, the range of $K_{D/W}$ is set in the same way as the type1 and the maximum value of $K_{L/U}$ is changed to 5.0. The range of design factors and sampling interval are shown in Table 1.

The CCD is used in this paper, and the estimation of performance is doable by plotting several response surfaces [16]. Fig. 12 shows two contour maps with respect to $K_{D/W}$ and $K_{L/U}$. The starting torque and current are shown in Fig. 12(a) and 12(b), respectively. The starting torque and current of the reference model are presented by red and orange solid lines on the contour maps, respectively. Also, the directions of increasing torque and decreasing current are indicated by yellow arrows. As $K_{D/W}$ increases, both torque and current increase as shown in Fig. 12(a). As $K_{L/U}$ increase, torque increases significantly compared to current. Hence, $K_{D/W}$ has a dominant influence on the starting current and the starting torque is affected by both $K_{D/W}$ and $K_{L/U}$.

The requirement of starting performances is different

Table 1. Range of design factors for response surface methodology.

Design factors	Range	Sampling interval
$K_{D/W}$	0.5-2.0	0.5
$K_{L/U}$	0.5-5.0	0.5

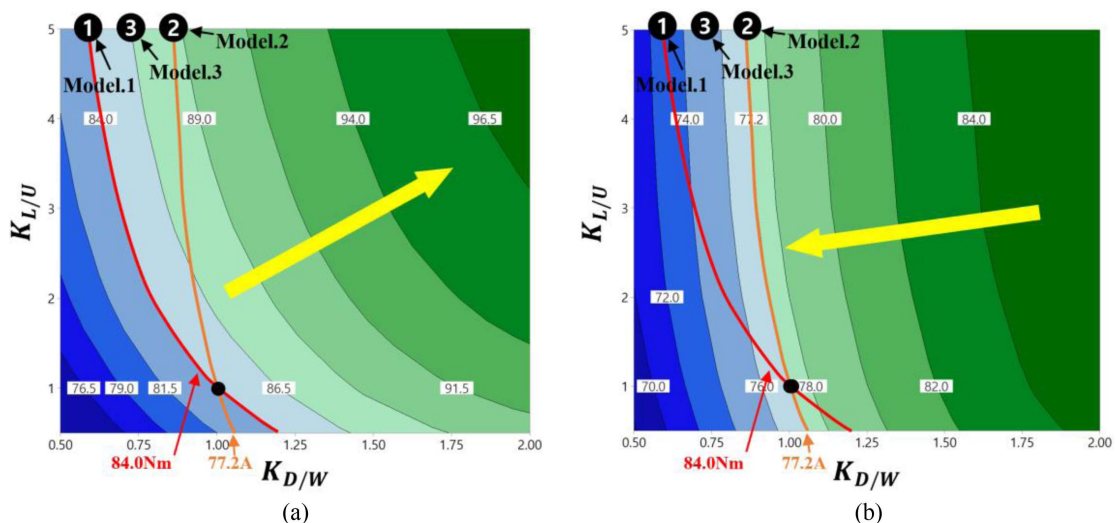






Fig. 12. (Color online) Contour maps on starting performances: (a) starting torque; (b) starting current.

Table 2. Comparisons of proposed models.

		Unit	Reference model	Model 1	Model 2	Model 3
	Shape	-				
	$K_{D/W}$	-	1.00	0.59	0.86	0.72
	$K_{L/U}$	-	1.00	5.00	5.00	5.00
Starting (CCD)	Torque	Nm	84.0	84.0	88.5	86.4
	Current	A	77.2	72.8	77.2	75.1
Starting (FEA)	Torque	Nm	84.0	84.3	88.9	86.7
	Current	A	77.2	73.1	77.7	75.6
Error rate (CCD vs FEA)	Torque	%	-	0.3	0.5	0.3
	Current	%	-	0.5	0.7	0.7
Rating	Torque	Nm	29.8	29.5	29.8	29.6
	Current	A	10.7	10.7	10.7	10.7
	Efficiency	%	92.1	92.0	92.0	92.0

depending on applications using a motor, and this paper proposes three models having improved starting performances as follows.

- 1) model 1 having same starting torque and the minimum starting current
- 2) model 2 having the maximum starting torque and same starting current
- 3) model 3 having increased starting torque and decreased starting current

The characteristic of the starting and rated operation for the reference model and selected three models are arranged in Table 2. In this table, there are two results on starting characteristic obtained from CCD and FEA, respectively, and all error rate between those data is under 1 %. The model 1 having the minimum starting current have same starting torque with the reference model, and starting current is 5.3 % decreased from 77.2A to 73.1A. The model 2 having the maximum torque has same starting current with the reference model, and starting torque is 5.8 % increased from 84.0Nm to 88.9Nm. In case of the model 3, starting torque is 3.1% increased and starting current is 2.1 % decreased in comparison with the reference model.

5. Conclusion

In this paper, it is confirmed that the two ratios for starting bar are key factors in varying the starting performance in a double squirrel cage IM. The current

distribution varies by the change the reactance and resistance with respect to the bar depth, and starting performance is determined by this distribution. When the depth decreases and the width increases, both the resistance and reactance of a rotor is reduced, and, as a result, the starting torque and current is significantly increased. On the other hand, when the width of the upper part is larger than the lower part, the reactance is decreased but the resistance is increased. For this reason, the starting torque is greatly increased by 6.7 % compared to the 2 % increased current.

The new shape in a starting bar having the characteristics of two ratios is proposed, and three models with improved starting performances are designed by using this shape. In case of the proposed models compared to the reference model, the starting torque has been increased by up to 5.8 % and the starting current has been decreased by up to 5.3 %. Also, torque, current, and efficiency for those models are the same as the reference model at the rated speed.

Acknowledgment

This research was supported by Korea Electric Power Corporation (Grant number: R19XO01-12) and Basic Science Research Program through the National Research Foundation of Korea funded by the Ministry of Education (Grant number: NRF-2018R1D1A1B07049717).

References

- [1] National Electrical Manufacturers Association. Energy management guide for selection and use of fixed frequency medium AC squirrel-cage polyphase induction motors. (2007).
- [2] J. Park, B. Kim, J. Yang, S. B. Lee, E. J. Wiedenbrug, M. Teska, and S. Han, IEEE Energy Conversion Congress and Exposition, 2493 (2010).
- [3] J. Antonino-Daviu, M. Riera-Guasp, J. Pons-Llinares, J. Park, S. B. Lee, J. Yoo, and C. Kral, IEEE Trans. Ind. Appl. **48**, 1539 (2012).
- [4] K. N. Gyftakis, D. Athanasopoulos, and J. Kappatou, International Conference on Electrical Machines, 1450 (2012).
- [5] D. H. Kim, J. H. Choi, K. S. Kim, J. Lee, and W. H. Kim, IEEE Trans. Appl. Super. **30**, 1 (2020).
- [6] D. H. Kim, K. S. Kim, J. Lee, I. J. Yang, S. W. Song, and W. H. Kim, IEEE Energy Conversion Congress and Exposition, 2042 (2020).
- [7] K. J. Park, K. Kim, S. H. Lee, D. H. Koo, K. C. Ko, and J. Lee, International Conference on Electrical Machines and Systems, 61 (2008).
- [8] B. Miroshnitschenko, F. Poltschak, and W. Amrhein, International Symposium on Power Electronics, 454 (2022).
- [9] S. Yamamoto, H. Hirahara, A. Tanaka, and T. Ara, IEEE Energy Conversion Congress and Exposition, 301 (2017).
- [10] T. Delphin, Y. Lefèvre, F. Biais, M. Tunzini, and C. Henaux, International Conference on Electrical Machines, 65 (2014).
- [11] A. Boglietti, A. Cavagnino, and M. Lazzari, IEEE Trans. Ind. Elec. **58**, 3734 (2010).
- [12] G. Joksimović, International Conference on Electrical Machines, 513 (2016).
- [13] I. Boldea and S. A. Nasarm, CRC Press (2010).
- [14] T. A. Lipo, Introduction to AC Machine Design, Wisconsin Power Electronics Research Center, University of Wisconsin. Madison Wisconsin (1996).
- [15] J. Yun and S. B. Lee, IEEE Trans. Mag. **53**, 1 (2017).
- [16] Y. Choo, H. Hwang, J. Cho, C. Kim, J. Kim, S. H. Hwang, J. Y. Choi, and C. Lee, IEEE Trans. Mag. **55**, 1 (2019).